Smart Proof System Instructions

It is recommended that you read all instructions below; even if you are familiar with online review practices.

Using the Smart Proof system, proof reviewers can easily review the PDF proof, annotate corrections, respond to queries directly from the locally saved PDF proof, all of which are automatically submitted directly to **our database** without having to upload the annotated PDF.

- ✓ **Login into Smart Proof** anywhere you are connected to the internet.
- ✓ **Review the proof** on the following pages and mark corrections, changes, and query responses using the **Annotation Tools**.

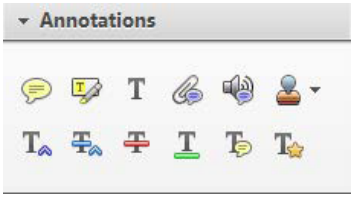

Note: Editing done by replacing the text on this PDF is not permitted with this application.

- ✓ **Save your proof corrections** by clicking the "Publish Comments" button.
  Corrections don't have to be marked in one sitting. You can publish comments and log back in at a later time to add and publish more comments before you click the "Complete Proof Review" button below.

- ✓ **Complete your review** after all corrections have been published to the server by clicking the "Complete Proof Review" button below.

Before completing your review.....

Did you reply to all author queries found in your proof?

Did you click the "Publish Comments" button to save all your corrections? Any unpublished comments will be lost.

Note: Once you click "Complete Proof Review" you will not be able to add or publish additional corrections.

JBC ARTICLE

Plant-derived mitochondria-targeting cysteine-rich peptide modulates cellular bioenergetics

Received for publication, November 17, 2018, and in revised form, January 7, 2019 Published, Papers in Press, January 23, 2019, DOI 10.1074/jbc.RA118.006693

Antony Kam[1], Shining Loo[1], Bamaprasad Dutta, Siu Kwan Sze, and James P. Tam[2]

From the School of Biological Sciences, Nanyang Technological University, 637551 Singapore

Edited by John M. Denu

Mitochondria are attractive therapeutic targets for developing agents to delay age-related frailty and diseases. However, few promising leads have been identified from natural products. Previously, we identified roseltide rT1, a hyperstable 27-residue cysteine-rich peptide from *Hibiscus sabdariffa*, as a knottin-type neutrophil elastase inhibitor. Here, we show that roseltide rT1 is also a cell-penetrating, mitochondria-targeting peptide that increases ATP production. Results from flow cytometry, live-cell imaging, pulldown assays, and genetically-modified cell lines supported that roseltide rT1 enters cells via glycosaminoglycan-dependent endocytosis, and enters the mitochondria through TOM20, a mitochondrial protein import receptor. We further showed that roseltide rT1 increases cellular ATP production via mitochondrial membrane hyperpolarization. Using biotinylated roseltide rT1 for target identification and proteomic analysis, we showed that human mitochondrial membrane ATP synthase subunit O is an intramitochondrial target. Collectively, these data support our discovery that roseltide rT1 is a first-in-class mitochondria-targeting, cysteine-rich peptide with potentials to be developed into tools to further our understanding of mitochrondria-related diseases.

Mitochondria, the main organelles regulating energy production, play vital roles in biosynthesis, intracellular signaling, and innate immunity (1–5). Mitochondrial dysfunction is the root cause of degenerative diseases, aging, and attendant aging issues, such as frailty and chronic inflammatory diseases (6–9). Emerging mitochondira-targeting strategies to slow the decline of mitochondrial functions showed promise in delaying the onset and reducing the severity of age-related diseases that increases the health span of aging populations (10–13).

Two primary strategies have been employed for designing mitochondria-targeting molecules. The first strategy exploits the biophysical and biochemical properties of the mitochondrial phospholipid bilayer and attendant strong negative membrane potential (−180 mV) (14). Cationic mitochondria-targeting molecules include guanidinium, triphenylphosphonium, and dequalinium moieties (14–18), and mitochondria-targeting oligopeptides (19–21), such as octa-arginine derivatives (22), D-(KLAKLAK)2 (23), and SS-31 (24–25). The second strategy exploits the mitochondrial protein import machinery, such as translocase of the outer membrane (TOM)[3] complexes (26). Most mitochondrial targeting sequences are rich in positively-charged and hydrophobic residues with amphipathic α-helical structures (27, 28). An example is the LSRLL presequence pentapeptide of rat aldehyde dehydrogenase, which adopts an amphipathic α-helical conformation upon binding to TOM20 (29–31).

Our laboratory has a long-standing interest in cysteine-rich peptides (CRPs) from plants, a class of naturally-occurring hyperstable constrained peptides (32–35). Plant CRPs of 2–6 kDa are highly under-represented as therapeutics or as leads for developing therapeutics in natural product research. Most CRPs are structurally compact and metabolically stable (32, 34) due to their evolutionarily conserved disulfide scaffolds and signature intercysteine loops that are hypervariable in sequence and size (32–33). Importantly, these loops often contain functional sequences that contribute to their biological activities (32, 36).

To date, there is no report of a naturally occurring plant-derived CRP with mitochondria-targeting properties. Previously, we identified roseltide rT1 from *Hibiscus sabdariffa* as a knottin-type neutrophil elastase inhibitor (32). Roseltide rT1 shares certain biophysical features similar to mitochondria-targeting molecules and Leu/Ile-rich helical peptides. It is positively-charged, has a Leu/Ile-rich sequence with 85% hydrophobic amino acids residues (Fig. S1), and four inter-cysteine loops that form a structure that resembles a four-leaf clover. Thus, roseltide rT1 could represent a novel class of naturally occurring mitochondria-targeting CRPs (mtCRP) with no sequence homology or structural similarity to known mitochondria-targeting helical peptides.

Herein, we show that roseltide rT1 is a cell-penetrating peptide that targets mitochondria and increases ATP production.

This work was supported in part by Competitive Research Grant NRF-CRP8-2011-05 from the National Research Foundation in Singapore, Nanyang Technological University Internal Funding-Synzymes and Natural Products (SYNC), and AcRF Tier 3 Grant MOE2016-T3-1-003. The authors declare that they have no conflicts of interest with the contents of this article.

This article contains Figs. S1–S13, Videos S1 and S2, and Datasets 1 and 2.

[1] Both authors contributed equally to the results of this work.

[2] To whom correspondence should be addressed: School of Biological Sciences, Nanyang Technological University, 60 Nanyang Dr., 637551 Singapore. E-mail: JPTam@ntu.edu.sg.

[3] The abbreviations used are: TOM, translocase of the outer membrane; CRP, cysteine-rich peptide; mtCRP, mitochondria-targeting CRPs; Fmoc, *N*-(9-fluorenyl)methoxycarbonyl; NHS, *N*-hydroxysuccinimide; HUVEC, human umbilical vein endothelial cells; FCCP, carbonyl cyanide 4-(trifluoromethoxy)phenylhydrazone; GFP, green fluorescent protein; TMRE, tetramethylrhodamine; ACN, acetonitrile; DCFH-DA, 2′-7′-dichlorodihydrofluorescein diacetate; TOCSY, total correlated spectroscopy; NOESY, nuclear Overhauser effect/enhancement spectroscopy; DMEM, Dulbecco's modified Eagle's medium; Tricine, *N*-[2-hydroxy-1,1-bis(hydroxymethyl)ethyl]glycine.

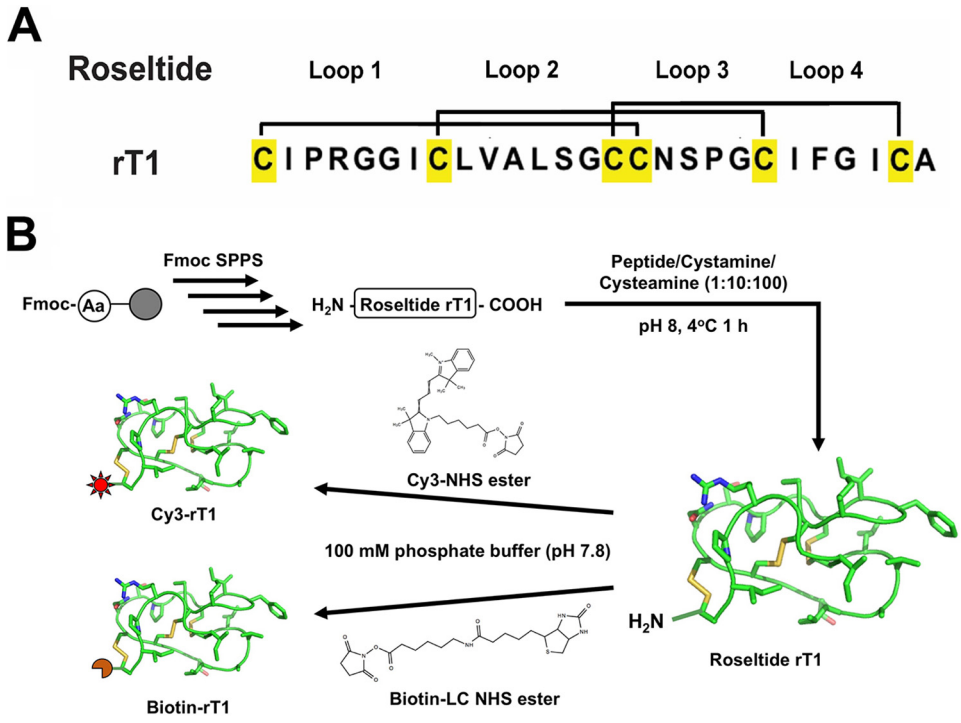

Figure 1. Synthesis and labeling of roseltide rT1. *A,* the primary structure of roseltide rT1. *B,* synthetic scheme for roseltide rT1 by solid-phase peptide synthesis, as well as biotinylation and fluorescent labeling of roseltide rT1.

Using interactomic analysis, we also identified ATP synthase subunit O as the putative intramitochondrial binding partner of roseltide rT1. Our findings highlight the characterization of a first-in-class, hyperstable, plant-derived mtCRP, which represents a promising lead to increase the health span of aging populations.

Results

Chemical synthesis and characterization of roseltide rT1

To avoid ambiguity from contaminants, particularly small molecules from plant extracts during isolation of native roseltide rT1, only the synthetic version of roseltide rT1 was used in the current work (Fig. 1). Synthetic roseltide rT1 was prepared by stepwise solid-phase synthesis using Fmoc chemistry. Deprotection and trifluoroacetic acid (TFA) cleavage released the linear roseltide rT1 precursor from the resin support. The linear precursor was immediately subjected to oxidative folding in 0.1 M ammonium bicarbonate at pH 8.0 in a mixture of redox agents, cysteamine/cystamine and 10% dimethyl sulfoxide (DMSO) for 1 h at 4 °C to give an overall yield of 50%. Further purification using reversed-phase (RP) high-performance LC (HPLC) resulted in a final peptide purity of >90%. Natural and synthetic roseltide rT1 were identical as determined by MALDI-TOF mass spectrometry (MS), co-elution by RP-HPLC, and overlay of their two-dimensional NOESY spectra (Figs. S2 and S3).

Cellular uptake of roseltide rT1

Roseltide rT1 is both positively charged and hydrophobic, properties commonly found in cell-penetrating peptides (37, 38). To determine the cellular uptake of roseltide rT1, flow cytometry and live-cell confocal microscopy were used. Roseltide rT1, which does not contain a lysine, was site-specifically conjugated at its N terminus using cyanine 3 (Cy3)-*N*-hydroxysuccinimide (NHS) ester. Cy3-labeled roseltide rT1 (Cy3-rT1) was purified by RP-HPLC and its identity confirmed using MALDI-TOF MS (Fig. S4). Flow cytometry was used to quantitatively measure the cellular uptake of Cy3-rT1 in human lung fibroblasts (WI-38) and human umbilical vein endothelial cells (HUVEC-CS). Incubation with 1 μM Cy3-rT1 in both cell lines resulted in increased fluorescence intensity of the cell population and reached a plateau in 1 h (Fig. 2*A*). Similar results were obtained from lymphocytes (Jurkat) and monocytes (THP-1) (Fig. S5), suggesting that cellular uptake of Cy3-rT1 is not cell-type specific. Live-cell imaging via confocal microscopy was used to prevent artifacts in the localization of labeled peptides in fluorescence microscopy (37). Fig. 2*B* shows an orthogonal view of the Z-stacked live-cell images of HUVEC-CS cells after incubation with 1 μM Cy3-rT1 for 15 min. The confocal images showed that Cy3-rT1 was internalized and distributed throughout the cell with no accumulation in the nucleus.

Cellular uptake of Cy3-rT1 is glycosaminoglycan-dependent

Roseltide rT1 contains a positively charged residue in loop 1 that could bind to negatively charged glycosaminoglycans. To determine whether glycosaminoglycan expression facilitates cellular uptake of roseltide rT1 at the extracellular matrix (39), we compared glycosaminoglycan-deficient mutant PgsA-745 cells with WT CHO-K1 cells as a control. Both cell lines were incubated with Cy3-rT1 for different durations of time, up to 30 min. Fig. 2*C* shows that CHO-K1 cells internalized Cy3-rT1 in a time-dependent manner, and the mean fluorescence intensity

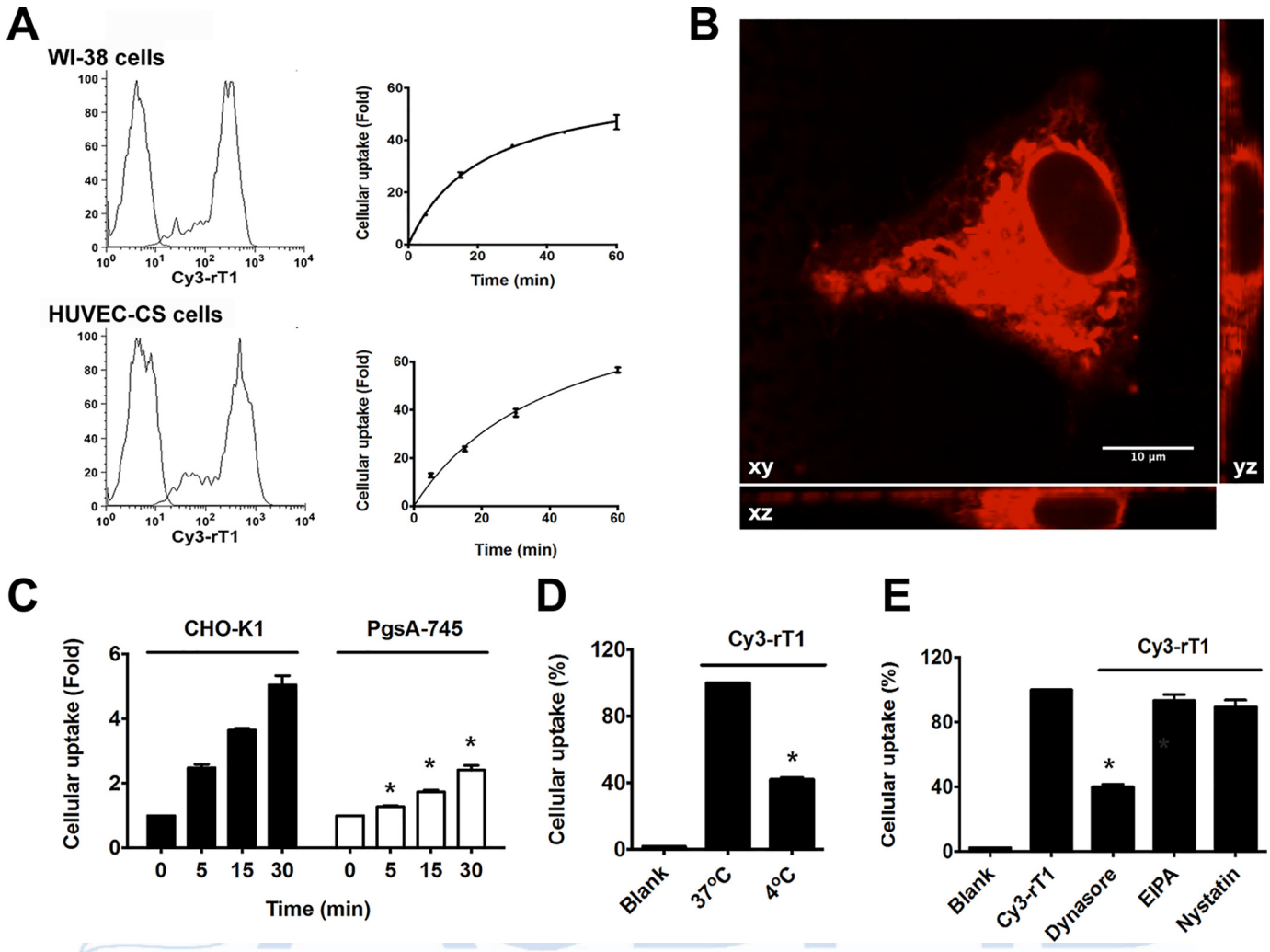

Figure 2. Cellular uptake of Cy3-rT1 is glycosaminoglycan- and endocytosis-dependent. *A,* flow cytometry analysis of WI-38 and HUVEC-CS cells after incubation with 1 μM Cy3-rT1 at 37 °C. *B,* Z-stack of HUVEC-CS cells after incubation with 1 μM Cy3-rT1 using live-cell confocal microscopy at 37 °C. *C,* flow cytometry analysis of CHO-K1 (WT) and PgS-A745 (glycosaminoglycan-deficient) cells after incubation with 1 μM Cy3-rT1 at 37 °C. *D,* flow cytometry analysis of HUVEC-CS cells incubated at 4 °C for 30 min before incubation with 1 μM Cy3-rT1 at 4 °C for 1 h. *E,* flow cytometry analysis of HUVEC-CS cells pretreated with endocytosis inhibitors dynasore, ethylisopropylamiloride (*EIPA*; 50 μM), and nystatin (50 μg/ml) for 30 min, followed by incubation with 1 μM Cy3-rT1 at 37 °C for 1 h. $n = 3$; $p < 0.05$ compared with control.

at different time points was significantly higher than that of Cy3-rT1-treated PgsA-745 cells ($p < 0.05$).

Endocytosis mediates cellular uptake of Cy3-rT1

To determine whether the mechanism of Cy3-rT1 cellular uptake is mediated by endocytosis, Cy3-rT1 was incubated with HUVEC-CS cells at 4 °C for 1 h. Fig. 2*D* shows that Cy3-rT1 cellular uptake was substantially reduced compared with uptake at 37 °C. These results suggested that the majority cellular uptake of Cy3-rT1 involves energy-dependent endocytosis. To further support the involvement of endocytosis in the cellular uptake of Cy3-rT1, HUVEC-CS cells were preincubated with different endocytosis inhibitors for 30 min before being incubated with Cy3-rT1 for 1 h. The results showed that the dynamin-dependent endocytosis inhibitor dynasore inhibited cellular uptake of Cy3-rT1, supporting the involvement of clathrin-mediated endocytosis, but not receptor- and caveolin-mediated endocytosis (Fig. 2*E*).

Cy3-rT1 is delivered to the mitochondrial compartment

To determine the subcellular localization of Cy3-rT1, we used organelle-specific fluorescent trackers to carry out colocalization experiments with live-cell confocal microscopy. Fig. 3*A* shows that Cy3-rT1 colocalized with MitoTracker Green FM, suggesting Cy3-rT1 escaped from endosomes and relocalized to the mitochondria. As a control, roseltide rT7, a hydrophilic rT1-homolog that was also isolated from *H. sabdariffa*, was fluorescently labeled with Cy3-NHS ester (Cy3-rT7). Confocal microscopic analysis showed that hydrophilic rT7 does not colocalize with MitoTracker Green FM. To further support colocalization experiments, N-terminal biotinylated roseltide rT1 (biotin-rT1) was incubated with HUVEC-CS cells for 1 h. The resultant mixture was then subjected to mitochondria isolation experiments, and immunoblot results showed that biotin-rT1 accumulated in the mitochondrial fraction (Fig. 3*B*).

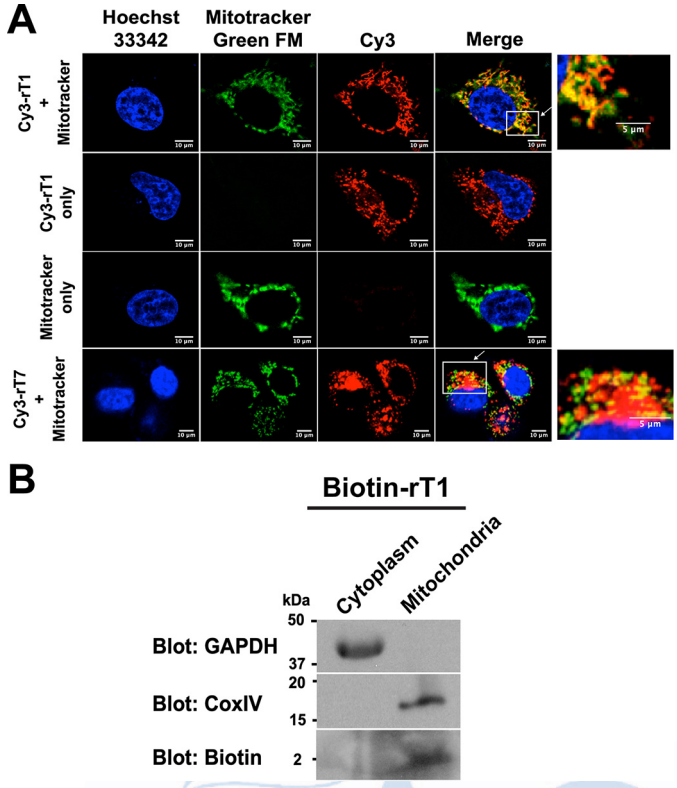

Figure 3. Cy3-rT1 localize to mitochondria upon internalization. *A*, 1 μM Cy3-rT1 colocalized with MitoTracker Green FM-labeled mitochondria according to live-cell confocal microscopy. 1 μM Cy3-rT7 alone was used as a negative control. *B*, Western blot analysis of 20 μM biotin-rT1–treated HUVEC-CS cells after separation of cytoplasmic and mitochondrial fractions using magnetic-activated cell sorting. Glyceraldehyde-3-phosphate dehydrogenase (*GAPDH*) was used as a cytoplasmic marker. Cytochrome *c* oxidase (*COX*) IV was used as a mitochondrial marker.

Identification of TOM20 as an intracellular target of roseltide rT1 for mitochondrial localization

The TOM family is involved in the mitochondria-targeting properties of signal peptides, especially TOM20 (40). To determine whether Leu/Ile-rich roseltide rT1 could interact with TOM20, we modeled their interactions using rigid body docking on the ClusPro version 2.0 server. Fig. 4*A* shows the X-ray crystal structure of the cytosolic domain of rat mitochondrial protein import receptor TOM20 (PDB entry 2V1T, chain A) (41). Based on this crystal structure, the four helices in the cytosolic domain of TOM20 form a hydrophobic groove that was reported to be the binding site for the pre-sequence peptide of rat aldehyde dehydrogenase (41). Fig. 4*A* shows the predicted computer model interaction of the leucine-rich intercysteine loop 2 of roseltide rT1 with the hydrophobic groove of TOM20. In support of modeling results, a pulldown assay followed by immunoblot with a TOM20 antibody showed that biotin-rT1 interacts with TOM20 (Fig. 4*B*, Fig. S6). To confirm these results *in vitro*, we established a TOM20-green fluorescent protein (GFP) stably transfected HEK293 cell line for colocalization experiments using live-cell confocal microscopy. The results showed that Cy3-rT1 colocalized with TOM20-GFP *in vitro* (Fig. 4*C*, Videos S1 and S2) and that mitochondria uncoupler carbonyl cyanide 4-(trifluoromethoxy)phenylhydrazone (FCCP) did not inhibit the mitochondrial localization properties of Cy3-rT1 (Fig. 4*D*). Using CRISPR-CAS9–mediated genome editing, we disrupted the mitochondrial protein expression of TOM20 in HepG2 cells (Fig. S7) and showed that Cy3-rT1 localization with MitoTracker Green FM was reduced compared with the control (Fig. 4*E*).

Effects of roseltide rT1 on mitochondrial function

Because roseltide rT1 targets mitochondria intracellularly, we examined its effect on mitochondrial function. Using Seahorse XF Cell Mito Stress assays, we determined the effects of roseltide rT1 on mitochondrial respiration. The results showed that roseltide rT1 does not significantly change the overall oxygen consumption rate of HepG2 cells. Treatment with roseltide rT1 showed a reduction in the FCCP-induced oxygen consumption rate, which is a mitochondria uncoupler that induces uncontrolled oxygen consumption (Fig. 5*A*). This suggested that roseltide rT1 affects mitochondria function. Simultaneously, roseltide rT1 did not affect the extracellular acidification rate (Fig. S8). To gain further insight into the mitochondrial effects of roseltide rT1, intact mitochondria were isolated and assayed with tetramethylrhodamine (TMRE) staining. The results demonstrated that roseltide rT1 induced hyperpolarization of the mitochondrial membrane in a dose-dependent manner, similar to mitochondrial hyperpolarization inducer oligomycin (Fig. 5*B*, Fig. S9). Additionally, roseltide rT1 increased reactive oxygen species levels in a dose-dependent manner using 2′-7′-dichlorodihydrofluorescein diacetate (DCFH-DA) staining (Fig. 5*C*). Using an ATP bioluminescent assay, roseltide rT1 increased the mitochondrial ATP level, whereas the effect can be inhibited by the mitochondria-uncoupling agent (Fig. 5*D*). Using C2C12 and HepG2 cells, roseltide rT1 increased cellular ATP levels in a dose-dependent manner (Fig. 5, *E* and *F*). Roseltide rT7 was used as a negative control that showed no significant changes in cellular ATP levels in HepG2 cells (Fig. S10).

Roseltide rT1 interacts with mitochondrial ATP synthase machinery

To identify the binding partners of roseltide rT1, pulldown assays followed by liquid chromatography (LC)-MS/MS analysis was performed to search for potential binding targets related to roseltide rT1 mitochondrial functions. After subtracting proteins found in control experiments, a total of 202 proteins were uniquely identified in the roseltide rT1 pulldown samples from which 86 proteins were discovered with multiple peptides (Dataset 1). The proteins DNA-J heat shock protein family 40 member C3, ATP synthase subunit 5O (ATP5O), and centrosomal protein 112 were identified in all three experimental repeats (Dataset 1). Fig. 6*A* shows the peptide sequence of ATP5O identified by LC-MS/MS analysis (Dataset 2). To confirm LC-MS/MS results, a pulldown assay was performed followed by Western blotting. Western blotting results supported the interaction between roseltide rT1 and ATP5O (Fig. 6*B*, Fig. S11). By measuring the reverse reaction of complex V as an ATPase, roseltide rT1 was not found to affect complex V activity (Fig. S12). Interestingly, incubation of roseltide rT1 in isolated intact mitochondria causes the dissociation of sirtuin 3 (SIRT3), an ATP5O-binding partner, from the ATP synthase

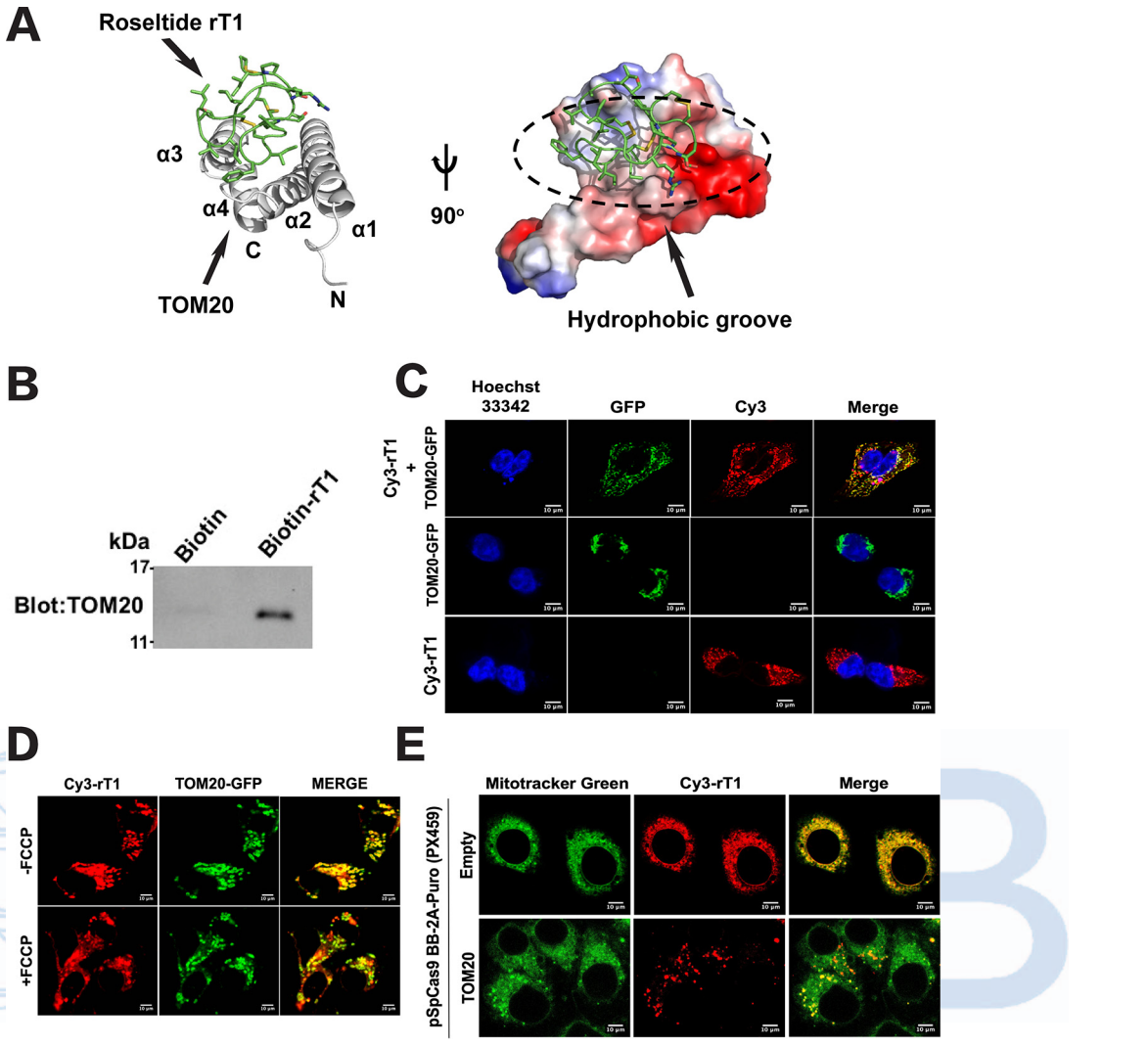

Figure 4. Roseltide rT1 interacts with TOM20 for mitochondrial localization. *A*, modeling the interaction between roseltide rT1 and TOM20 (PDB entry 2V1T) using the ClusPro Version 2.0 server. *B*, Western blot analysis using a TOM20 antibody revealed that biotin-rT1 binds to TOM20. *C*, Cy3-rT1 colocalizes with TOM20-GFP in stably-transfected HEK293 cells according to live-cell confocal microscopy. *D*, co-incubation of 1 μM Cy3-rT1 with 1 μM mitochondria uncoupler FCCP, did not block the mitochondrial localization properties of Cy3-rT1 according to live-cell confocal microscopy. *E*, depletion of TOM20 in HepG2 cells by CRISPR/CAS9 reduced the mitochondrial localization of Cy3-rT1 according to live-cell confocal microscopy.

complex (Fig. 6*C*). This suggests that roseltide rT1 can promote SIRT3-mediated deacetylation in the mitochondria.

Discussion

Mitochondria are important therapeutic targets for delaying the onset of aging and age-related diseases (1, 2, 6, 8, 9). Substantial efforts have been made to design and develop novel mitochondria-targeting molecules that include small molecules and peptides (15, 19–21, 25–27). Recently, there has been increasing interest in peptide-based therapeutics due to their ease of synthesis, tunability, and biocompatibility (42–46). Currently, the majority of mitochondria-targeting peptides designed are partly based on mitochondria-targeting sequences that are invariably rich in positively-charged and hydrophobic residues and adopt amphipathic α-helical conformations (21, 27). The present study reports the first naturally occurring plant-derived mtCRP, which represents a novel class of nonhelical, hyperstable mitochondria-targeting compound with a four-loop "clover-like" structure that is formed by three disulfide bonds.

Roseltide rT1 possesses an evolutionarily conserved cystine-knot disulfide connectivity and a four-looped structural-fold (32). Based on our previously reported *in silico* model, we speculated that the intercysteine loop 1 of roseltide rT1 is responsible for its inhibitory activities against human neutrophil elastase (32). Functional roles of the other loops, however, were not determined. To broaden our understanding of the functional spectrum of roseltide rT1, solid-phase peptide synthesis and chemical biology were utilized to determine its intracellular functions. Amine-reactive chemistry using NHS ester was performed to prepare fluorescent- and biotin-labeled roseltide rT1 (Cy3-rT1 and biotin-rT1, respectively). Cy3-rT1 was observed to bind and internalize into a variety of cell lines, including fibroblasts (WI-38), endothelial cells (HUVEC-CS), hepatocytes (Hep-G2), lymphocytes (Jurkat), and monocytes (THP-1). Additionally, internalization of Cy3-rT1 was significantly reduced in glycosaminoglycan-deficient cells (PgsA-745) compared with WT (CHO-K1). These findings suggested that the cell-penetrating properties of roseltide rT1 are not cell-type

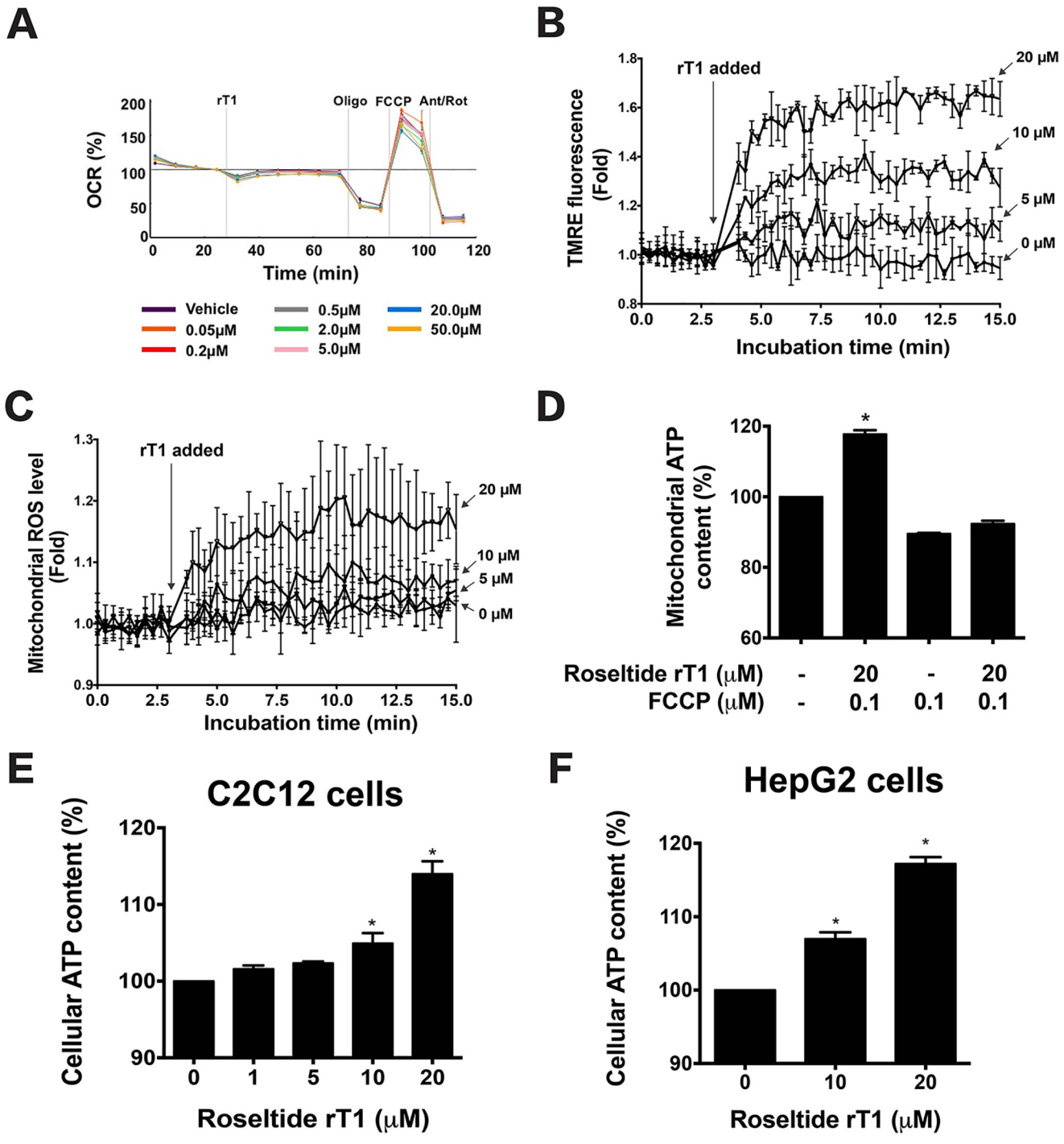

Figure 5. Effects of roseltide rT1 on mitochondrial function. *A*, oxygen consumption rate (*OCR*) profile of HepG2 cells after incubation with roseltide rT1 via Seahorse XFe96 Flux Analyzer. *B*, effects of roseltide rT1 on mitochondrial membrane potential using TMRE-stained, isolated, intact mitochondria from HepG2 cells. *C*, effects of roseltide rT1 on mitochondria reactive oxygen species levels (*ROS*) using DCFH-DA–stained, isolated, intact mitochondria from HepG2 cells. *D*, effects of roseltide rT1 on mitochondrial ATP content using isolated, intact mitochondria from HepG2 cells. $n = 3$; *, $p < 0.05$ compared with blank. Effects of roseltide rT1 on cellular ATP level in C2C12 (*E*) and HepG2 (*F*) cells. $n = 3$; *, $p < 0.05$ compared with control.

specific but dependent on the expression of glycosaminoglycans at the extracellular matrix. As glycosaminoglycans are highly negatively charged molecules (47), we speculated that the positively charged intercysteine loop 1 of roseltide rT1 was responsible for its binding.

Direct cell penetration and endocytosis are two primary mechanisms involved in the cellular uptake of cell-penetrating peptides (38, 48). Our results showed that cellular uptake of Cy3-rT1 was temperature-dependent and sensitive to the endocytosis inhibitor dynasore, supporting our findings that Cy3-rT1 penetrates cells through dynamin-dependent endocytosis mechanisms. Upon cellular entry, Cy3-rT1 was shown to localize in the mitochondria using live-cell confocal microscopy and subcellular fractionation. Eukaryotes have thousands of mitochondrial proteins that are mostly synthesized as precursors with cleavable N-terminal presequences (mitochondri-

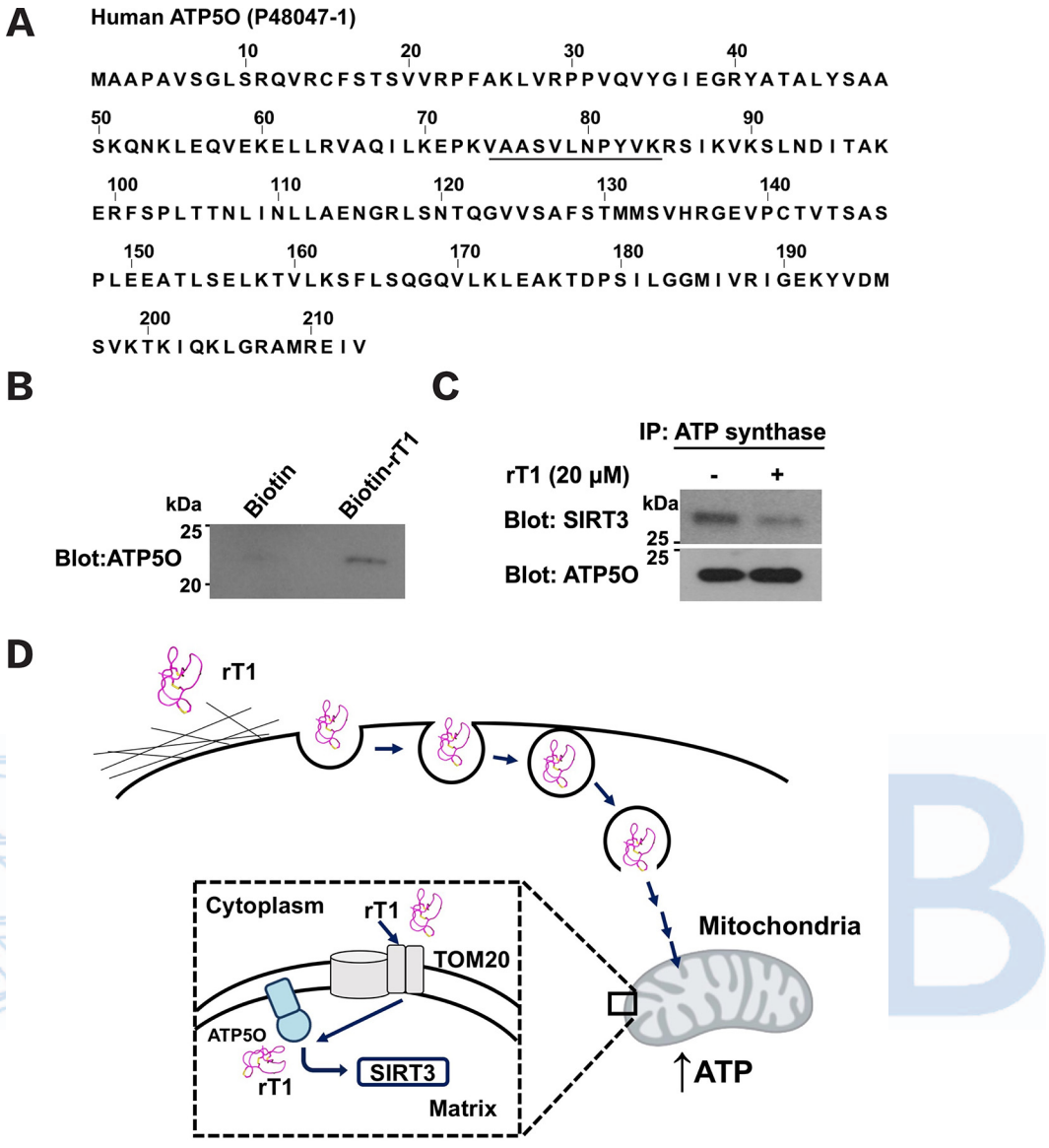

Figure 6. Roseltide rT1 interacts with ATP5O. *A,* peptide sequence (*underlined*) identified from the full sequence of ATP5O using interactomic analysis by LC-MS/MS. *B,* Western blot analysis using an ATP5O antibody revealed that biotin-rT1 binds to ATP5O. *C,* incubation of roseltide rT1 (20 μM) with isolated intact mitochondria from HepG2 cells disassociated SIRT3 from ATP synthase according to Western blot analysis following ATP synthase immunoprecipitation.

a-targeting sequences). An example is the presequence peptide of rat liver aldehyde dehydrogenase (49). These mitochondria-targeting sequences are often recognized by the first protein import receptor at the outer membrane of mitochondria (*i.e.* TOM20) (50). Previous studies demonstrated that leucine residues of the pre-sequence peptide of rat aldehyde dehydrogenase are essential for binding to TOM20 (49). The consensus binding motif of TOM20 is $\phi 1X2X3\phi 4\phi 5$ (ϕ = hydrophobic amino acids, X = any amino acids) (41). Because the primary sequence of roseltide rT1 has >85% hydrophobic residues and is Leu/Ile-rich, TOM20 poses as its potential intracellular target. Rigid surface modeling of the protein–protein interactions between roseltide rT1 and TOM20 were performed in this study. The leucine-rich intercysteine loop 2 of roseltide rT1 was predicted to interact with the hydrophobic groove formed by the four α-helices (α1–α4) of TOM20. In support of our predictions, pulldown assays showed the interaction of roseltide rT1 with TOM20, and confocal microscopy revealed the colocalization of Cy3-rT1 with TOM20-GFP live cells. Moreover, depletion of TOM20 significantly reduced the localization of Cy3-rT1 in the mitochondria. Taken together, these findings suggest that roseltide rT1 interacts with TOM20 and accumulates in the mitochondria.

Mitochondria produce >90% of the total cellular energy available, and defects in energy metabolism are a common cause of aging and age-related diseases (51–53). Results from the Seahorse XF Cell Mito Stress assay showed that roseltide rT1 affects mitochondrial function. Interestingly, roseltide rT1 was resistant to FCCP (mitochondria uncoupler)-induced uncontrolled oxygen consumption. It also triggered mitochondria hyperpolarization and reactive oxygen species generation, suggesting mitochondrial oxygen-dependent ATP synthesis, resulting in an overall increase in cellular ATP production. These results were in contrast to the classical effects of chemi-

cal entities (*e.g.* hydrogen peroxide (54)) that affect FCCP-induced oxygen consumption rates.

Interatomic analysis of roseltide rT1 identified ATP5O as its putative intramitochondrial target. ATP5O, commonly known as oligomycin-sensitive conferral protein, is the δ-subunit of human mitochondrial F_1F_0-ATP synthase (55). Located at the peripheral stalk, ATP5O plays a vital role in tethering F_1 and F_0, and holding the F_1 subunits together (55). Roseltide rT1 showed no effects on the ATP hydrolysis activities of ATP synthase, which suggests that the observed mitochondrial effects of roseltide rT1 were not due to a direct effect on ATP synthase activity but an indirect effect related to the binding partners of ATP5O (Fig. S12).

Recently, Yang *et al.* (56) reported SIRT3 as a ATP5O-binding partner. 50% of the mitochondrial proteome was reported to be acetylated and SIRT3 was found to be an NAD^+-dependent protein deacetylase (56). Upon mitochondrial membrane depolarization by an uncoupler, SIRT3 dissociates from ATP5O and deacetylates electron transport chain complexes (56). This results in increased electron transport efficiency, restoration of the proton gradient, and promotion of oxidative metabolism (56). This phenomenon was suggested to be an acute response to stress and provides fast recovery of mitochondrial function (56). Because roseltide rT1 binds to ATP5O, have counteractive effects against FCCP, and increases ATP production, it is possible that roseltide rT1 facilitates the dissociation of SIRT3 from ATP5O. This unique mechanism results in proton gradient generation and increased ATP production. Thus, we proposed that the mitochondrial functions of roseltide rT1 are, at least in part, a result of its putative role as a binding partner of ATP5O (Fig. 6*D*). Future studies are warranted to explore the relationship between the functions of roseltide rT1 and mitochondrial acetylation.

In conclusion, this study reports the chemical synthesis of roseltide rT1 and demonstrated its energy-dependent endocytic cell-penetrating properties. Upon cellular entry, roseltide rT1 interacts with TOM20 and binds to ATP5O, resulting in an increased ATP production. Taken together, these findings highlight roseltide rT1 as a first-in-class naturally occurring mtCRP with the potentials to be developed into a mitochondrial therapeutic.

Experimental procedures

Materials

All chemicals and solvents were purchased from Sigma, and ThermoFisher Scientific, unless specified otherwise.

Extraction and purification of roseltide rT1

Dried calyces (1 kg) of *H. sabdariffa* were extracted with water and centrifuged at 9000 rpm for 10 min at 4 °C (Beckman Coulter). The supernatant was filtered and the filtrate loaded onto a C18 flash column (Grace Davison, USA) and eluted with 60% ethanol, 0.01% TFA. The eluted fractions were loaded onto an SP-Sepharose resin column (GE Healthcare, UK) and eluted with 1 M NaCl (pH 3.0), followed by ultrafiltration (ViVaflow 200, 2000 molecular weight cut-off hydrostat). Further purification was done by RP-HPLC (Shimadzu, Japan). A linear gradient of mobile phase A (0.05% TFA in H_2O) and mobile phase B (0.05% TFA in acetonitrile (ACN)) was used with the C18 column (250 × 22 mm, 5 μm, 300Å; Grace Davison, USA). MALDI-TOF MS was used to identify the presence of roseltide rT1 in the eluted fractions.

Chemical synthesis and oxidative folding of roseltide rT1

Roseltide rT1 was synthesized by Fmoc-based solid-phase peptide synthesis on Wang resin. The peptide was cleaved in a cleavage mixture (92.5% TFA, 2.5% H_2O, 2.5% 1,2-ethanedithiol, and 2.5% triisopropylsilane) at room temperature for 2 h. The crude cleaved product was folded in 10% dimethyl sulfoxide (DMSO), 90% 0.1 M NH_4HCO_3 (pH 8.0), cystamine (10 eq), and cysteamine (100 eq) for 1 h at 4 °C. Folded roseltide rT1 was purified by preparative HPLC (250 × 21 mm, 5 μm; Phenomenex). A linear gradient of mobile phase A (0.1% TFA in H_2O) and mobile phase B (0.1% TFA in ACN) was used. The folding yield was ~50%. RP-HPLC and two-dimensional NMR were performed to compare the physical properties of synthetic roseltide rT1 to its native form (Figs. S2 and S3).

Site-specific N-terminal fluorescent labeling of roseltide rT1

Synthetic roseltide rT1 was fluorescently labeled with Cy3 using NHS ester (Lumiprobe, USA) in 100 mM phosphate buffer (pH 7.8). Fluorescent labeling was carried out at room temperature for 16 h, and Cy3-rT1 was then identified and purified by RP-HPLC and MALDI-TOF MS (Fig. S4).

Site-specific N-terminal biotinylation of roseltide rT1

Synthetic roseltide rT1 was biotinylated with EZ-Link NHS-LC-biotin in 100 mM phosphate buffer (pH 7.8). Biotinylation was carried out at room temperature for 2 h, and biotin-rT1 was identified and purified by MALDI-TOF MS and RP-HPLC (Fig. S13).

NMR spectroscopy

Natural and synthetic rT1 for NMR spectroscopy was prepared by dissolving the lyophilized peptide in d_6-DMSO containing at a final peptide concentration of 1 mM. All NMR spectra were collected at a sample temperature of 298 K on a Bruker AVANCE II 600 MHz NMR spectrometer equipped with four RF channels and a 5-mm Z-gradient TCI cryoprobe. Phase-sensitive two-dimensional $^1H,^1H$-TOCSY and NOESY spectra were recorded with a spectral width of 12 ppm. For water suppression, excitation sculpting with gradients was applied to all NMR experiments. TOCSY and NOESY spectra were obtained with mixing times of 80 and 200 ms, respectively. All measurements were recorded with 2048 complex data points and zero-filled to 2048 × 512 data matrices. Time domain data in both dimensions were multiplied by a 90° shifted squared sine bell window function prior to Fourier transformation. Baseline correction was applied with a fifth order polynomial. NMR data were acquired and processed by TopSpin (Bruker BioSpin). The NMR spectra were processed with NMRFAM-Sparky.

Cell culture

WI-38, HUVEC-CS, C2C12, and HepG2 cells were cultured in Dulbecco's modified Eagle's medium (DMEM) supplemented with 10% fetal bovine serum and 100 units/ml of peni-

cillin and streptomycin. THP-1 and Jurkat cells were cultured in Roswell Park Memorial Institute (RPMI) 1640 medium supplemented with 10% fetal bovine serum and 100 units/ml of penicillin and streptomycin. CHO-K1 and mutant PgsA-745 CHO-K1 cells (deficient in xylosyltransferase) were cultured in DMEM/Ham's F-12 medium containing 15 mM HEPES, L-glutamine, 10% fetal bovine serum, and 100 units/ml of penicillin and streptomycin and grown in a 5% CO_2 humidified incubator at 37 °C. HEK293 cells were stably transfected with a TOM20-GFP plasmid (kindly provided by Prof. Li Yu of Tsinghua University, Beijing, China) by electroporation and selected using 500 μg/ml of G418 in DMEM supplemented with 10% fetal bovine serum and 100 units/ml of penicillin and streptomycin. To generate CRISPR/Cas9-engineered HepG2 cells with depleted TOM20 expression, the TOM20 CRISPR guide RNA sequence (5′-TAAGCTCCCAACAATTAGTC-3′) was cloned into the pSpCas9 BB-2A-Puro (PX459) version 2.0 vector by GenScript (USA). The genetically-modified cells were obtained by electroporation and selected using 10 μg/ml of puromycin, DMEM supplemented with 10% fetal bovine serum and 100 units/ml of penicillin and streptomycin. TOM20 expression was verified by Western blotting following mitochondria isolation (Fig. S7).

Cellular uptake analyses by flow cytometry

To study the cellular uptake of Cy3-rT1 by flow cytometry, cells were incubated with 1 μM Cy3-rT1 in serum-free medium at 37 °C. Following incubation, cells were harvested and collected by centrifugation at 500 × *g* for 5 min. To quench extracellular fluorescence, cells were treated with 150 μg/ml of trypan blue, and the samples were analyzed by flow cytometry. A total of 10,000 cells were analyzed using a BD LSRFortessa™ X-20 flow cytometer. For temperature-dependent uptake studies, HUVEC-CS cells were incubated at 4 °C for 30 min prior to incubation with Cy3-rT1 for 1 h at 4 °C. For endocytosis inhibitor studies, HUVEC-CS cells were pretreated with endocytosis inhibitors, including dynasore (50 μM), ethylisopropylamiloride (50 μM), and nystatin (50 μg/ml) for 30 min, followed by incubation with Cy3-rT1 for 1 h at 37 °C.

Confocal microscopy analysis

To examine the intracellular distribution of Cy3-rT1, cells were seeded on an 8-well chamber slide (Ibidi, Germany). Prior to incubation with Cy3-rT1, cells were stained with Hoechst 333241. Cy3-rT1 was incubated on cells in phenol red-free and serum-free medium at 37 °C. The slides were washed gently with phosphate-buffered saline (PBS) three times, and the media was replaced prior to imaging. Slides were observed using a Zeiss LSM 710 confocal microscope. For certain experiments, cells were stained with MitoTracker Green FM (100 nM) for 15 min before incubating with Cy3-rT1 (1 μM) for 15 min.

Mitochondria isolation using magnetically activated cell sorting

Mitochondria were isolated from HepG2 cell lysates using anti-TOM22 magnetic microbeads according to the manufacturer's instruction (Miltenyl Biotec, Germany). Briefly, mitochondria were labeled with anti-TOM22 microbeads in separation buffer for 1 h at 4 °C. The suspension was then passed through a 30-μm filter and loaded onto an LS column. After washing the column with separation buffer, intact mitochondria were eluted using elution buffer.

Localization of roseltide rT1 by subcellular fractionation

HUVEC-CS cells were incubated with 20 μM biotin-rT1 in serum-free medium at 37 °C. Following incubation, the cells were subjected to mitochondria isolation using magnetically-activated cell sorting. The cytoplasmic and mitochondrial fractions were resolved using Novex™ 10–20% Tricine gels (Life Technologies) at 100 V for 120 min.

Pulldown assay

Pulldown assay was performed using NeutrAvidin UltraLink Resin. Briefly, the resin was washed with PBS three times and incubated with biotin-rT1 or biotin alone (control) at room temperature with rotation for 2 h. Bovine serum albumin (BSA; 2%) in PBS was added to both tubes and incubated at room temperature with gentle end-over-end mixing for another 2 h. HUVEC-CS cell lysate (600 μg) was added to each tube and allowed to incubate overnight at 4 °C with rotation. After incubation, the resin was transferred to Pierce® Spin columns and washed 10 times with PBS. Then, 6× loading dye with β-mercaptoethanol was added to the resin and heated for 10 min at 85 °C. The resultant mixture was centrifuged at 200 × *g* for 1 min and resolved using 15% SDS-PAGE at 100 V for 120 min.

Immunoprecipitation of ATP synthase complex V

Isolated intact mitochondria were incubated with roseltide rT1 (20 μM) for 15 min, then ATP synthase complex V was immunoprecipitated using an ATP Synthase Immunocapture kit (Abcam). Briefly, mitochondria were lysed using lauryl maltoside. After centrifugation at 21,000 × *g* for 10 min at 4 °C, the supernatant was incubated with solid beads overnight at 4 °C with rotation. The beads were then washed with wash buffer twice and eluted with 50 μl of 1% SDS. The eluted fraction was mixed with 6× loading dye with β-mercaptoethanol and heated for 10 min at 85 °C. The resultant mixture was centrifuged at 14,000 × *g* for 1 min and resolved using 12% SDS-PAGE at 100 V for 120 min.

Western blotting

Blot transfer onto a polyvinylidene difluoride membrane (GE Healthcare, Sweden) was performed at 250 mA for 120 min on ice. The blot was blocked with 5% BSA in TBS and Tween 20 (TBST) before incubating overnight at 4 °C with a mouse anti-TOM20 (1:200 in 5% BSA-TBST; Santa Cruz Biotechnology), mouse anti-glyceraldehyde-3-phosphate dehydrogenase (1:5,000 in 5% BSA-TBST; Avivas Systems Biology), rabbit anti-cytochrome *c* oxidase IV (1:2,000 in 5% BSA-TBST; Cell Signaling Technology), mouse anti-oligomycin sensitivity conferring protein (1:200 in 5% BSA-TBST; Santa Cruz Biotechnology), mouse anti-SIRT3 (1:200 in 5% BSA-TBST; Santa Cruz Biotechnology), and neutravidin-horseradish peroxidase (1:10,000 in 5% BSA-TBST; Life Technologies) antibodies. After overnight incubation, the membrane was washed with TBST at

room temperature three times for 10 min each. The blot was then incubated with secondary mouse or rabbit anti-horseradish peroxidase (1:5000 in 5% BSA-TBST; Cell Signaling Technology) for 1 h at room temperature. The blot was washed five times for 10 min each with TBST at room temperature before addition of chemiluminescence substrate (Advansta, USA) and exposure on X-ray film (Fujifilm, Japan).

Sample preparation and in-gel digestion for LC-MS/MS

Experimental and control samples from pulldown assays were resolved by 15% SDS-PAGE at 100 V for 120 min. Each sample lane was cut and sliced into three fractions according to their molecular weight. The gel pieces were reduced with 10 mM DTT for 30 min at 60 °C and alkylated with 55 mM iodoacetamide in the dark for 45 min at room temperature. The alkylated samples were subjected to tryptic digestion (Promega) at 37 °C overnight. Tryptic peptides were then extracted with 5% acetic acid, 50% ACN buffer and evaporated by vacuum centrifuge (Thermo Electron).

LC-MS/MS

LC-MS/MS analysis was performed using an online Dionex UltiMate 3000 UHPLC system coupled with an Orbitrap Elite mass spectrometer (Thermo Scientific Inc., Germany). Tryptic peptides were dissolved in 0.1% formic acid solution and separated by a Acclaim PepMap RSL column (75 μm inner diameter, 15 cm, 2 μm particle size) using a 60-min gradient of mobile phase A and mobile phase B (0.1% formic acid in 90% ACN). Samples were sprayed through a Michrom Thermo Captive Spray nanoelectrospray ion source (Bruker-Michrom Inc.) with a source voltage of 1.5 kV. A full MS scan range was set at 350–1600 m/z and resolution of 60,000 at 400 m/z. The Fourier transform-MS/MS scan range was set at 150–2000 m/z, with a resolution of 15,000 at 400 m/z. The 10 most intense ions with a threshold of 500 counts were selected for high-energy collisional dissociation fragmentation and fragmented using 32% normalized collision energy with a maximum ion accumulation time of 120 ms. Parameters including an automatic gain control of 1E+06 for the full MS scan and 2E+05 for the MS/MS scan, active precursor ion charge state screening, and capillary temperature of 250 °C were set for the experiment. Data acquisition was conducted in positive mode using LTQ Tune Plus software.

LC-MS/MS data analyses

Mascot generic format files were generated from the raw data using Proteome Discoverer 1.4.1.14 software prior to Mascot searching. All protein sequence database searches were performed on the in-house Mascot search engine (version 2.4.1; Matrix Science, UK) using the UniProt Knowledge Base human database along with the reverse sequences (downloaded on March 2016, including 3,47,018 sequences and 121,280,492 residues). Carbamidomethyl at cysteine was set as a static modification and methionine oxidation and asparagine/glutamine deamidation as dynamic modifications. Full trypsin digestion with a maximum of 2 missed and/or nonspecific cleavages was set as the digestion parameter. 10 ppm for precursor mass and 0.02 Da for fragment mass were set as mass tolerance parameters. The #13C value of 2 was set as other search parameter. Data with a significance threshold value of $p < 0.05$ and "Ignore Ions Score Below" value of 20 were extracted in *csv format. A target-decoy search strategy with the cutoff set to less than 1% false discovery rate and proteins identified with multiple peptides were applied for the selection of proteins for final analysis. The exponentially modified protein abundance index value for each identified protein was calculated by Mascot and used for label-free quantification.

Oxygen consumption and extracellular acidification rates

A Seahorse Bioscience Mito stress test kit was used to determine the oxygen consumption and extracellular acidification rates as per the manufacturer's instructions (Seahorse Bioscience). Briefly, HepG2 cells were treated with roseltide rT1, and extracellular oxygen levels and pH were measured in real time using an XFe96 Flux Analyzer (Seahorse Bioscience) by Cyprotex Discovery, Ltd. (UK).

Mitochondrial membrane potential

Mitochondrial membrane potential was determined using TMRE staining of isolated intact mitochondria. Briefly, 0.1 mg of isolated mitochondria from HepG2 cells were incubated with TMRE (200 nM) for 15 min. Then, mitochondria were incubated with roseltide rT1, and fluorescent intensity was measured using a microplate reader at 549 nm excitation and 575 nm emission wavelengths (Tecan Infinite® 200 Pro, Switzerland).

Mitochondrial reactive oxygen species levels

Mitochondrial reactive oxygen species levels were determined using DCFH-DA staining of isolated intact mitochondria. Briefly, 0.1 mg of isolated mitochondria from HepG2 cells were incubated with DCFH-DA (10 μM) for 10 min. Then, mitochondria were incubated with roseltide rT1, and fluorescent intensity was measured using a microplate reader at 485 nm excitation and 520 nm emission wavelengths (Tecan Infinite® 200 Pro, Switzerland).

ATP bioluminescent assay

Cellular ATP levels were determined using a CellTiter-Glo® luminescent cell viability assay as per the manufacturer's instructions (Promega). Briefly, C2C12 and HepG2 cells were incubated with roseltide rT1 for 4 h, and 100 μl of CellTiter-Glo® reagent was added to each well. Roseltide rT7 was used as negative control. For ATP measurement in isolated intact mitochondria from magnetically activated cell sorting, isolated mitochondria were incubated with roseltide rT1 with/without FCCP for 1 h, and 100 μl of CellTiter-Glo® reagent was added to each well. Following incubation, the luminescent intensity was measured using a microplate reader (Tecan Infinite® 200 Pro, Switzerland).

Mitochondria isolation by reagent-based method

To examine the mitochondrial protein expression of TOM20 in HepG2 cells after CRISPR-CAS9-mediated genome editing, mitochondria were isolated using a commercial mitochondria isolation kit (reagent-based method) according to manufacturer's instructions (ThermoFisher).

ATP synthase (complex V) activity

The effects of roseltide rT1 on ATP synthase (complex V) enzyme activity were determined using a commercial ATP synthase specific activity microplate assay kit according to the manufacturer's instructions (Abcam).

In silico modeling

The *in silico* docking was performed using automatic protein–protein docking server ClusPro version 2.0 (57, 58). To model the interactions between roseltide rT1 and TOM20, both the NMR structure of roseltide rT1 (PDB entry 5GSF) and the crystal structure of the cytosolic domain of rat TOM20 (PDB entry 2V1T) (59) were uploaded to the server. It uses a rigid body docking protocol, and the model was generated based on both electrostatic potentials and hydrophobic interactions.

Statistical analyses

Statistical comparisons were performed using GraphPad version 6.0d (USA). The data were analyzed by one-way analysis of variance followed by Newman-Keuls post hoc test. Data are expressed as the mean ± S.E. $p < 0.05$ was considered statistically significant.

Author contributions—A. K. and S. L. formal analysis; A. K., S. L., B. D., and J. P. T. investigation; A. K., S. L., and J. P. T. writing-original draft; A. K., S. L., and J. P. T. writing-review and editing; S. K. S. and J. P. T. supervision; S. K. S. validation; J. P. T. conceptualization; J. P. T. resources; J. P. T. funding acquisition; J. P. T. project administration.

References

1. Galluzzi, L., Kepp, O., Trojel-Hansen, C., and Kroemer, G. (2012) Mitochondrial control of cellular life, stress, and death. *Circ. Res.* **111,** 1198–1207 CrossRef Medline
2. McBride, H. M., Neuspiel, M., and Wasiak, S. (2006) Mitochondria: more than just a powerhouse. *Curr. Biol.* **16,** R551-R560 CrossRef Medline
3. Folmes, C. D., Dzeja, P. P., Nelson, T. J., and Terzic, A. (2012) Metabolic plasticity in stem cell homeostasis and differentiation. *Cell Stem Cell* **11,** 596–606 CrossRef Medline
4. Sahin, E. (2010) Depinho, R. A., Linking functional decline of telomeres, mitochondria and stem cells during ageing. *Nature* **464,** 520–528 CrossRef Medline
5. Parker, G. C., Acsadi, G., and Brenner, C. A. (2009) Mitochondria: determinants of stem cell fate? *Stem Cells Dev.* **18,** 803–806 CrossRef Medline
6. Salvioli, S., Bonafè, M., Capri, M., Monti, D., and Franceschi, C. (2001) Mitochondria, aging and longevity: a new perspective. *FEBS Lett.* **492,** 9–13 CrossRef Medline
7. Weber, T. A., and Reichert, A. S. (2010) Impaired quality control of mitochondria: aging from a new perspective. *Exp. Gerontol.* **45,** 503–511 CrossRef Medline
8. Balaban, R. S., Nemoto, S., and Finkel, T. (2005) Mitochondria, oxidants, and aging. *Cell* **120,** 483–495 CrossRef Medline
9. Chan, D. C. (2006) Mitochondria: dynamic organelles in disease, aging, and development. *Cell* **125,** 1241–1252 CrossRef Medline
10. de Cavanagh, E. M., Inserra, F., Ferder, L., and Angiotensin, I. I. (2011) Blockade: a strategy to slow ageing by protecting mitochondria? *Cardiovasc. Res.* **89,** 31–40 Medline
11. Dumont, M., and Beal, M. F. (2011) Neuroprotective strategies involving ROS in Alzheimer disease. *Free Radic. Biol. Med.* **51,** 1014–1026 CrossRef Medline
12. Cheng, Z., and Ristow, M. (2013) Mitochondria and metabolic homeostasis. Vol. 19, Mary Ann Liebert, Inc., New Rochelle, NY CrossRef
13. Suomalainen, A. (2011) Therapy for mitochondrial disorders: little proof, high research activity, some promise. *Semin. Fetal Neonatal Med.* **16,** 236–240
14. Sheu, S.-S., Nauduri, D., and Anders, M. W. (2006) Targeting antioxidants to mitochondria: a new therapeutic direction. *Biochim. Biophys. Acta* **1762,** 256–265 CrossRef Medline
15. Zhang, X. Y., and Zhang, P. Y (2016) Mitochondria targeting nano agents in cancer therapeutics. *Oncol. Lett.* **12,** 4887–4890 CrossRef Medline
16. Huang, J. G., Leshuk, T., and Gu, F. X. (2011) Emerging nanomaterials for targeting subcellular organelles. *Nano Today* **6,** 478–492 CrossRef
17. Ross, M. F., Kelso, G. F., Blaikie, F. H., James, A. M., Cocheme, H. M., Filipovska, A., Da Ros, T., Hurd, T. R., Smith, R. A., and Murphy, M. P. (2005) Lipophilic triphenylphosphonium cations as tools in mitochondrial bioenergetics and free radical biology. *Biochemistry* **70,** 222–230 Medline
18. Weiss, M. J., Wong, J. R., Ha, C. S., Bleday, R., Salem, R. R., Steele, G. D., and Chen, L. B. (1987) Dequalinium, a topical antimicrobial agent, displays anticarcinoma activity based on selective mitochondrial accumulation. *Proc. Natl. Acad. Sci. U.S.A.* **84,** 5444–5448 CrossRef Medline
19. Yousif, L. F., Stewart, K. M., Horton, K. L., and Kelley, S. O. (2009) Mitochondria-penetrating peptides: sequence effects and model cargo transport. *ChemBioChem.* **10,** 2081–2088 CrossRef Medline
20. Yousif, L. F., Stewart, K. M., and Kelley, S. O. (2009) Targeting mitochondria with organelle-specific compounds: strategies and applications. *ChemBioChem.* **10,** 1939–1950 CrossRef Medline
21. Horton, K. L., Stewart, K. M., Fonseca, S. B., Guo, Q., and Kelley, S. O. (2008) Mitochondria-penetrating peptides. *Chem. Biol.* **15,** 375–382 CrossRef Medline
22. Kloss, A., Henklein, P., Siele, D., Schmolke, M., Apcher, S., Kuehn, L., Sheppard, P. W., and Dahlmann, B. (2009) The cell-penetrating peptide octa-arginine is a potent inhibitor of proteasome activities. *Eur. J. Pharm. Biopharm.* **72,** 219–225 CrossRef Medline
23. Ellerby, H. M., Arap, W., Ellerby, L. M., Kain, R., Andrusiak, R., Rio, G. D., Krajewski, S., Lombardo, C. R., Rao, R., Ruoslahti, E., Bredesen, D. E., and Paswualini, R. (1999) Anti-cancer activity of targeted pro-apoptotic peptides. *Nat. Med.* **5,** 1032–1038 CrossRef Medline
24. Szeto, H. H. (2008) Cell-permeable, mitochondrial-targeted, peptide antioxidants. *Drug Addiction*, pp. 535–546, Springer, New York
25. Szeto, H. H. (2006) Mitochondria-targeted peptide antioxidants: novel neuroprotective agents. *AAPS J.* **8,** E521-E531 CrossRef Medline
26. Hoshino, A., Fujioka, K., Oku, T., Nakamura, S., Suga, M., Yamaguchi, Y., Suzuki, K., Yasuhara, M., and Yamamoto, K. (2004) Quantum dots targeted to the assigned organelle in living cells. *Microbiol. Immunol.* **48,** 985–994 CrossRef Medline
27. von Heijne, G. (1986) Mitochondrial targeting sequences may form amphiphilic helices. *EMBO J.* **5,** 1335–1342 CrossRef Medline
28. Lemire, B. D., Fankhauser, C., Baker, A., and Schatz, G. (1989) The mitochondrial targeting function of randomly generated peptide sequences correlates with predicted helical amphiphilicity. *J. Biol. Chem.* **264,** 20206–20215 Medline
29. Thornton, K., Wang, Y., Weiner, H., and Gorenstein, D. (1993) Import, processing, and two-dimensional NMR structure of a linker-deleted signal peptide of rat liver mitochondrial aldehyde dehydrogenase. *J. Biol. Chem.* **268,** 19906–19914 Medline
30. Hammen, P. K., Waltner, M., Hahnemann, B., Heard, T. S., and Weiner, H. (1996) The role of positive charges and structural segments in the presequence of rat liver aldehyde dehydrogenase in import into mitochondria. *J. Biol. Chem.* **271,** 21041–21048 CrossRef Medline
31. Wang, Y., and Weiner, H. (1993) The presequence of rat liver aldehyde dehydrogenase requires the presence of an α-helix at its N-terminal region which is stabilized by the helix at its C termini. *J. Biol. Chem.* **268,** 4759–4765 Medline
32. Loo, S., Kam, A., Xiao, T., Nguyen, G. K., Liu, C. F., and Tam, J. P. (2016) Identification and characterization of Roseltide, a knottin-type neutrophil elastase inhibitor derived from hibiscus sabdariffa. *Sci. Rep.* **6,** 39401 CrossRef Medline

33. Loo, S., Kam, A., Xiao, T., and Tam, J. P. (2017) Bleogens: cactus-derived anti-*Candida* cysteine-rich peptides with three different precursor arrangements. *Front. Plant Sci.* **8,** 2162 CrossRef Medline
34. Nguyen, P. Q., Wang, S., Kumar, A., Yap, L. J., Luu, T. T., Lescar, J., and Tam, J. P. (2014) Discovery and characterization of pseudocyclic cystine-knot α-amylase inhibitors with high resistance to heat and proteolytic degradation. *FEBS J.* **281,** 4351–4366 CrossRef Medline
35. Nguyen, P. Q., Luu, T. T., Bai, Y., Nguyen, G. K., Pervushin, K., and Tam, J. P. (2015) Allotides: proline-rich cystine knot α-amylase inhibitors from *Allamanda cathartica*. *J. Nat. Prod.* **78,** 695–704 CrossRef Medline
36. Nguyen, K. N., Nguyen, G. K., Nguyen, P. Q., Ang, K. H., Dedon, P. C., and Tam, J. P. (2016) Immunostimulating and Gram-negative-specific antibacterial cyclotides from the butterfly pea (*Clitoria ternatea*). *FEBS J.* **283,** 2067–2090 CrossRef Medline
37. Richard, J. P., Melikov, K., Vives, E., Ramos, C., Verbeure, B., Gait, M. J., Chernomordik, L. V., and Lebleu, B. (2003) Cell-penetrating peptides: a reevaluation of the mechanism of cellular uptake. *J. Biol. Chem.* **278,** 585–590 CrossRef Medline
38. Zorko, M., and Langel, Ü. (2005) Cell-penetrating peptides: mechanism and kinetics of cargo delivery. *Adv. Drug Deliv. Rev.* **57,** 529–545 CrossRef Medline
39. Pae, J., Liivamägi, L., Lubenets, D., Arukuusk, P., Langel, Ü., and Pooga, M. (2016) Glycosaminoglycans are required for translocation of amphipathic cell-penetrating peptides across membranes. *Biochim. Biophys. Acta* **1858,** 1860–1867 CrossRef Medline
40. Yamamoto, H., Itoh, N., Kawano, S., Yatsukawa, Y., Momose, T., Makio, T., Matsunaga, M., Yokota, M., Esaki, M., Shodai, T., Kohda, D., Hobbs, A. E., Jensen, R. E., and Endo, T. (2011) Dual role of the receptor Tom20 in specificity and efficiency of protein import into mitochondria. *Proc. Natl. Acad. Sci. U.S.A.* **108,** 91–96 CrossRef Medline
41. Saitoh, T., Igura, M., Obita, T., Ose, T., Kojima, R., Maenaka, K., Endo, T., and Kohda, D. (2007) Tom20 recognizes mitochondrial presequences through dynamic equilibrium among multiple bound states. *EMBO J.* **26,** 4777–4787 CrossRef Medline
42. Han, T. S., Teichert, R. W., Olivera, B. M., and Bulaj, G. (2008) Conus venoms: a rich source of peptide-based therapeutics. *Curr. Pharm. Des.* **14,** 2462–2479 CrossRef Medline
43. Craik, D. J., Fairlie, D. P., Liras, S., and Price, D. (2013) The future of peptide-based drugs. *Chem. Biol. Drug Des.* **81,** 136–147 CrossRef Medline
44. Jagadish, K., and Camarero, J. A. (2010) Cyclotides, a promising molecular scaffold for peptide-based therapeutics. *Pept. Sci.* **94,** 611–616 CrossRef
45. Garcia, E., and Camarero, J. A. (2010) Biological activities of natural and engineered cyclotides, a novel molecular scaffold for peptide-based therapeutics. *Curr. Mol. Pharmacol.* **3,** 153–163 CrossRef Medline
46. Otvos, L. (2008) Peptide-based drug design: here and now. *Methods Mol. Biol.* **494,** 1–8 CrossRef Medline
47. Snow, A. D., Willmer, J., and Kisilevsky, R. (1987) A close ultrastructural relationship between sulfated proteoglycans and AA amyloid fibrils. *Lab. Invest.* **57,** 687–698 Medline
48. Madani, F., Lindberg, S., Langel, U., Futaki, S., and Gräslund, A. (2011) Mechanisms of cellular uptake of cell-penetrating peptides. *J. Biophys.* **2011,** 414729 Medline
49. Wiedemann, N., Frazier, A. E., and Pfanner, N. (2004) The protein import machinery of mitochondria. *J. Biol. Chem.* **279,** 14473–14476 CrossRef Medline
50. Neupert, W., and Herrmann, J. M. (2007) Translocation of proteins into mitochondria. *Annu. Rev. Biochem.* **76,** 723–749 CrossRef Medline
51. Newmeyer, D. D., and Ferguson-Miller, S. (2003) Mitochondria: releasing power for life and unleashing the machineries of death. *Cell* **112,** 481–490 CrossRef Medline
52. Ferrari, R. (1996) The role of mitochondria in ischemic heart disease. *J. Cardiovasc. Pharmacol.* **28,** 1–10 CrossRef Medline
53. Szeto, H. H. (2008) Cell-permeable, mitochondrial-targeted, peptide antioxidants. *Drug Addiction*, pp. 535–546, Springer, New York
54. Armstrong, J. A., Cash, N. J., Ouyang, Y., Morton, J. C., Chvanov, M., Latawiec, D., Awais, M., Tepikin, A. V., Sutton, R., and Criddle, D. N. (2018) Oxidative stress alters mitochondrial bioenergetics and modifies pancreatic cell death independently of cyclophilin D, resulting in an apoptosis-to-necrosis shift. *J. Biol. Chem.* **293,** 8032–8047 CrossRef Medline
55. Chen, H., Morris, M. A., Rossier, C., Blouin, J.-L., and Antonarakis, S. E. (1995) Cloning of the cDNA for the human ATP synthase OSCP subunit (ATP5O) by exon trapping and mapping to chromosome 21q22.1-q22.2. *Genomics* **28,** 470–476 CrossRef Medline
56. Yang, W., Nagasawa, K., Münch, C., Xu, Y., Satterstrom, K., Jeong, S., Hayes, S. D., Jedrychowski, M. P., Vyas, F. S., Zaganjor, E., *et al.* (2016) Mitochondrial sirtuin network reveals dynamic SIRT3-dependent deacetylation in response to membrane depolarization. *Cell* **167,** 985–1000.e21 CrossRef Medline
57. Comeau, S. R., Gatchell, D. W., Vajda, S., Camacho, C. J. (2004) ClusPro: a fully automated algorithm for protein–protein docking. *Nucleic Acids Res.* **32,** W96-W99 CrossRef Medline
58. Comeau, S. R., Gatchell, D. W., Vajda, S., and Camacho, C. J. (2004) ClusPro: an automated docking and discrimination method for the prediction of protein complexes. *Bioinformatics* **20,** 45–50 CrossRef Medline
59. Navia, M. A., McKeever, B. M., Springer, J. P., Lin, T.-Y., Williams, H. R., Fluder, E. M., Dorn, C. P., and Hoogsteen, K. (1989) Structure of human neutrophil elastase in complex with a peptide chloromethyl ketone inhibitor at 1.84-Å resolution. *Proc. Natl. Acad. Sci. U.S.A.* **86,** 7–11 CrossRef Medline

AUTHOR QUERIES

AUTHOR PLEASE ANSWER ALL QUERIES 1

AQau—Please confirm the given-names and surnames are identified properly by the colours.
= Given-Name, = Surname
The colours are for proofing purposes only. The colours will not appear online or in print.

AQaff—Please confirm the following full affiliations or correct here as necessary. This is what will appear in the online HTML version:

School of Biological Sciences, Nanyang Technological University, 637551 Singapore

A—Au: Can you please confirm or correct the FundRef entries?

1.] Funder Name : Ministry of Education - Singapore (MOE)
Funder ID : http://search.crossref.org/fundref?q=501100001459
Grant ID : MOE2016-T3-1-003
Author(s) : Antony Kam, Shining Loo & Bamaprasad Dutta
Author(s) : Siu Kwan Sze & James P. Tam

2.] Funder Name : National Research Foundation Singapore (NRF)
Funder ID : http://search.crossref.org/fundref?q=501100001381
Grant ID : NRF-CRP8-2011-05
Author(s) : Antony Kam, Shining Loo & Bamaprasad Dutta
Author(s) : Siu Kwan Sze & James P. Tam

3.] Funder Name : Nanyang Technological University (NTU)
Funder ID : http://search.crossref.org/fundref?q=501100001475
Author(s) : Antony Kam, Shining Loo & Bamaprasad Dutta
Author(s) : Siu Kwan Sze & James P. Tam

B—Au: It is important that your article's funding information be correct in two places: 1. The footnote, on the first page of your article. 2. Your article's publication metadata, on the query sheet. This metadata is delivered to Crossref after publication and increases the discoverability of your article. Please confirm that the correct funding information is listed in BOTH #1 and #2 above. For #2, you only need check the funder names and grant numbers (we have already confirmed the URL). If there are any discrepancies, please tell us what needs to be corrected, so we can ensure your funding information is correct prior to final publication.

AUTHOR QUERIES

AUTHOR PLEASE ANSWER ALL QUERIES 2

C—Au: changed to Dataset 1, per Jnl style, numbers must be in sequential order

D—Au: changed to comma per Jnl style when number is used in mixture, under Exp proc, 60% ethanol, 0.01% TFA

E—Au: Should media be changed to medium? If only 1 medium was used then please change media to medium. Media is plural and means more than 1 medium. Under Exp proc

F—Au: According to Journal style, most abbreviations in the text must be used a minimum of 3 times, so "ANOVA" was spelled out throughout.

G—Au: please confirm all definitions in abbr footnote